Study of the cell reversal process of large area proton exchange membrane fuel cells under fuel starvation

Dong Liang [a,b], Qiang Shen [a,b], Ming Hou [a,*], Zhigang Shao [a], Baolian Yi [a]

[a] Fuel Cell System and Engineering Laboratory, Dalian Institute of Chemical Physics, Chinese Academy of Sciences, Dalian 116023, China
[b] Graduate University of Chinese Academy of Sciences, Beijing 100049,China

ABSTRACT

In this research, the fuel starvation phenomena in a single proton exchange membrane fuel cell (PEMFC) are investigated experimentally. The response characteristics of a single cell under the different degrees of fuel starvation are explored. The key parameters (cell voltage, current distribution, cathode and anode potentials, and local interfacial potentials between anode and membrane, etc.) are measured in situ with a specially constructed segmented fuel cell. Experimental results show that during the cell reversal process due to the fuel starvation, the current distribution is extremely uneven, the local high interfacial potential is suffered near the anode outlet, hydrogen and water are oxidized simultaneously in the different regions at the anode, and the carbon corrosion is proved to occur at the anode by analyzing the anode exhaust gas. When the fuel starvation becomes severer, the water electrolysis current gets larger, the local interfacial potential turns higher, and the carbon corrosion near the anode outlet gets more significant. The local interfacial potential near the anode outlet increases from ca. 1.8 to 2.6 V when the hydrogen stoichiometry decreases from 0.91 to 0.55. The producing rate of the carbon dioxide also increases from 18 to 20 ml min^{-1}.

Crown Copyright © 2009 Published by Elsevier B.V. All rights reserved.

1. Introduction

Proton exchange membrane fuel cell (PEMFC) is believed to be one of the most promising alternatives to the internal combustion engine for its low operation temperature, fast start-up time and favorable power-to-weight ratio, etc. Although PEMFCs have achieved significant progress in recent years, short lifetime is still one of the primary problems that should be overcome to enable its wide commercialization [1].

Fuel starvation, which could be a potential cause for the early failure of proton exchange membrane fuel cells (PEMFCs), usually occurs under harsh operating conditions such as sub-zero start-up and rapid load change with the high fuel utilization [2]. Uneven flow distribution caused by poorly designed flow field, stack or assembly structure would also induce local fuel starvation in a single cell or fuel starvation of some cells in a stack [3]. Under the fuel starvation conditions, hydrogen is no longer enough to be oxidized to maintain the current, so water electrolysis and carbon corrosion reaction would take place at the anode to provide the required protons and electrons for the oxygen reduction reaction at the cathode. The reactions are as follows:

$$2H_2O \rightarrow O_2 + 4H^+ + 4e^- \qquad (1)$$

$$C + 2H_2O \rightarrow CO_2 + 4H^+ + 4e^- \qquad (2)$$

The carbon corrosion reaction at the anode could weaken the attachment of Pt particles to the carbon support, decrease the electronic continuity of the catalyst layer, and eventually lead to severe Pt agglomeration and cell performance degradation.

The fuel starvation behavior of phosphoric fuel cell has been studied and reported by some researchers [4–7], but that of PEMFC is still needed to be well understood. Knights et al. [2] studied the polarization of fuel cell under a complete fuel starvation condition. The cell voltage drop was detected and the presence of oxygen at the anode was proved by GC. The reference hydrogen electrode (RHE) method was also used to study on the starvation behavior of PEM-FCs by a few researchers [8–10]. In the Taniguchi et al.'s work [8], the changes of cell voltage, the anode and cathode potentials against RHE with time were examined in situ, and uneven catalyst degradation was found. Localized anode and cathode electrode potentials against dynamic hydrogen reference electrodes were measured by Lauritzen et al. [9]. In their research, rather high localized corrosive electrochemical potential at the cathode was found and CO$_2$ was detected in the cathode exhaust. The current distribution method, being very effective in investigating the distribution properties of fuel cells [11–14], was employed by Liu et al. [3] to analyze the behaviors of PEMFC under reactant starvation. In their study, the overall cell polarizations and current distributions under hydrogen and air starvations were explored separately. "Vacuum effect" was shown to occur at the anode under hydrogen starvation condition,

* Corresponding author. Tel.: +86 411 84379051; fax: +86 411 84379185.
E-mail address: houming@dicp.ac.cn (M. Hou).

which was also reported by Kim et al. [15]. Instructive results were given in the above-mentioned works, but the process of cell reversal caused by fuel starvation of some cells in a stack was seldom investigated.

In this research, fuel starvation conditions of a single cell in a stack were simulated experimentally. Current distribution, anode and cathode potentials, and local interfacial potentials between anode and membrane were measured in order to reveal the cell reversal process further.

2. Experimental

2.1. Experimental system

To study the PEMFC starvation behavior, an experimental system (shown in Fig. 1) was constructed. It included a homemade fuel cell stack test station, a stack, a homemade single cell test station, a segmented single fuel cell and a data acquisition system. In the experimental system, the single cell was electrically connected with the stack. The operating conditions of the stack and the segmented cell were controlled individually. Fuel starvation was made intentionally by adjusting the gas stoichiometry of the segmented cell, so that the behavior of the single cell and the stack (even the interactions between them) under fuel starvation can be investigated. In this research, the process of the single segmented cell during fuel starvation is our main concern. In the following work, the interactions between the stack and the single cell will be studied further.

The homemade stack test station was used mainly to monitor each cell's voltage and control the operating conditions of the stack, such as pressure, temperature, gas flowrate and relative humidity. KIKUSUI PLZ2004 with four load boosters connected in parallel was used as the electronic load. The stack was made of 13 cells, and its structure was the same with that adopted in our previous work [14].

Homemade single cell test station was mainly used to control the operating conditions of the single cell individually. The gas flowrates were adjusted by digital-controlled mass flow controllers (D07 Series, Sevenstar). The reaction gases were humidified

by bubbling method, and their humidity levels were adjusted by controlling the dew point temperatures of the humidified gases. The cell temperature was controlled by adjusting the recirculating water temperature. Specially constructed segmented single cell was adopted to measure the responding characteristics of the single cell under fuel starvation. Its detailed structure would be illustrated in Section 2.2.

The specially constructed single cell testing and data acquisition system mainly included a 15-channel current collecting device, an 8-channel voltage collecting device and an 8-channel temperature collecting device. The current collecting device was made of a PCL-818 series multifunction card and a PCLD-8115 wiring terminal from Advantech Company connecting with 15 LEM LT58-S7 Hall elements. The voltage collecting device utilized PCI-1713 multifunction card from Advantech Company to collect in situ voltages of maximum 8 channels. The temperature collecting device collected maximum 8 channels of in situ temperatures through ADAM-4018 multifunction card from Advantech Company. All the above-mentioned data were recorded automatically by a PC with programmed software.

2.2. Single cell structure

To measure the current distribution and the local electrode potential, a special MEA and a cathode current collecting end plate were constructed to realize a segmented single cell structure. The cell structure is shown in Fig. 2. Components I, II, III are the anode end plate, the current collecting plate and the bipolar plate, respectively; IV is the specially designed MEA; V is the specially constructed segmented cathode end plate.

The MEA was specially designed as shown in Fig. 3, with gas diffusion electrodes (GDEs) as the electrodes and Pt/C as the catalyst. The Pt loading of catalyst at each side was $0.4 \, \text{mg cm}^{-2}$. The anode active area was $270 \, \text{cm}^2$ with normal structure. Static reference hydrogen electrode was designed at the hydrogen inlet of anode. The reference electrode was connected with normal reaction region through proton exchange membrane. During the experiments, fuel would firstly pass the reference hydrogen electrode
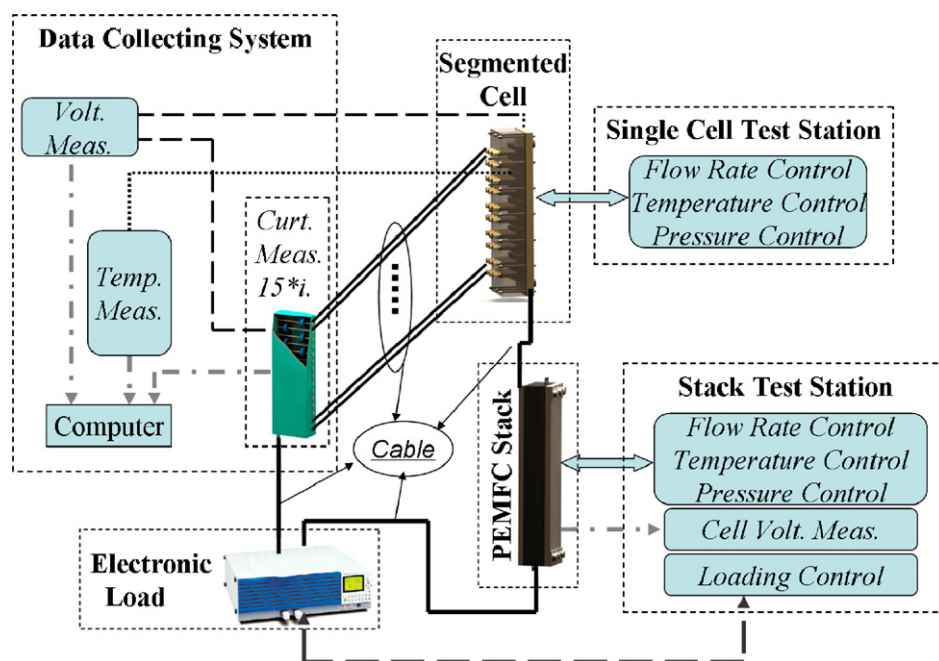

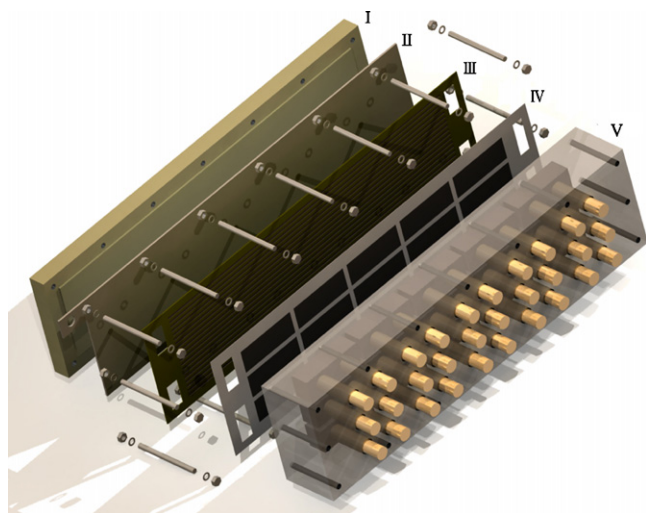**Fig. 1.** Experimental flow chart.

Fig. 2. Schematic of the segmented cell assembly (I, anode end plate; II, anode current collecting plate; III, anode flow field plate; IV, MEA; V, cathode end plate).

Fig. 4. Structure of the cathode current collecting end plate.

Table 1
Operating conditions of the segmented single cell.

No.	Total fuel flow rate (ml min^{-1})	Hydrogen stoichiometry
1	800	1.82
2	480	1.09
3	400	0.91
4	320	0.73
5	240	0.55

region at the anode inlet. The cathode electrode was segmented, the active area of each segment was 15.36 cm^2, and the total active area was 230.4 cm^2. The segments were numbered from 1 to 5 along the hydrogen flow direction. The proton exchange membrane used was two commercial Nafion® 212 membranes. Three voltage sensors were sandwiched between the two membranes in different regions. The voltage sensor was made of copper wire with insulating layer outside, and its diameter was about 80 μm. 2 mm insulating layer was removed at each end of the copper wire to make the voltage sensor conductive.

Fig. 4 shows the specially made cathode current collecting end plate. Fifteen graphite blocks were embedded in an organic glass plate uniformly in a matrix of 3 × 5 corresponding to the MEA segments. Flow fields were conventional parallel channel pattern and carved after milling. Silver plated copper sticks were adopted to collect the current of each segment.

With the specially designed segmented single cell, the current distribution, the cathode and anode potentials relative to static reference hydrogen electrode, and the local interfacial potentials between anode and membrane can be measured in situ during the experiments.
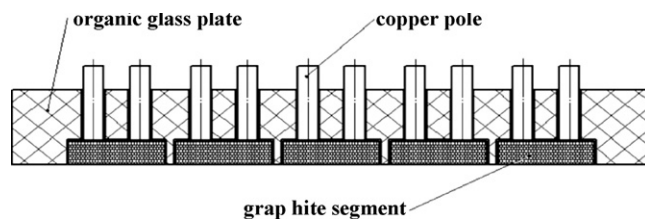
2.3. Experimental details

During the experiments, the stack was always kept at normal operating conditions to provide power for the single cell reversal. Reaction gases were air and pure hydrogen, and the operating pressures of them were maintained to be 0.05 MPa by back pressure valves. The hydrogen stoichiometry was 1.5, and the air stoichiometry was 2.5. They were both under saturated humidification. The stack temperature was controlled at 60 °C. The loading current was kept at 46 A, and the current density was 200 mA cm^{-2} with regard to the cathode effective active area of the segmented single cell.

The segmented single cell utilized the mixing gas of hydrogen and nitrogen (73% hydrogen plus 27% nitrogen) as the fuel, and air as the oxidant. The single cell temperature and the dew point temperatures of the humidified gases were all kept at 60 °C. Reaction gases were kept at ambient pressure and operated in co-flow mode. The exhaust hydrogen from the single cell and the stack were combined together after flowing through the back pressure valve. The air flowrate was fixed at 2.3 l min^{-1} (λ = 3.0), and the fuel flowrate varied. The detailed experimental conditions were listed in Table 1.
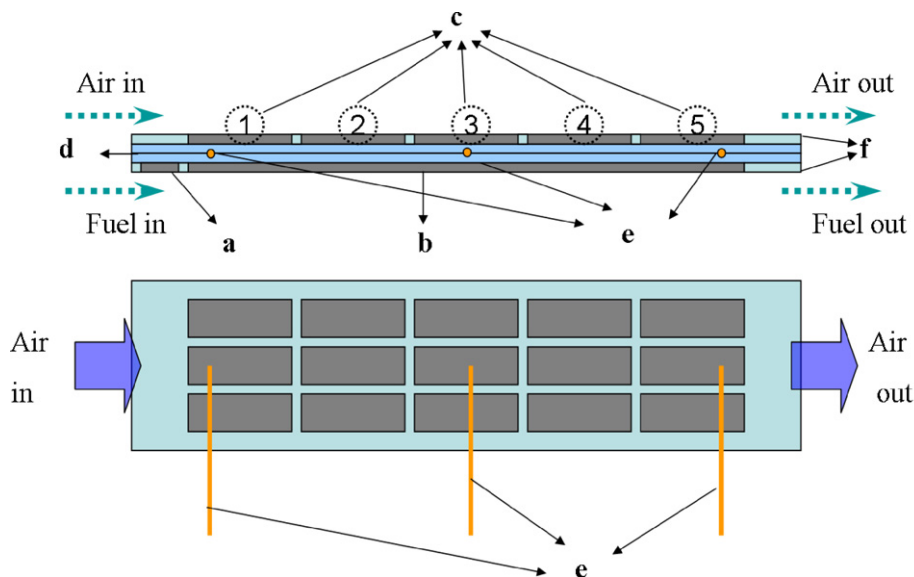

Fig. 3. Structure of the specially constructed MEA (a, reference hydrogen electrode; b, anode; c, segmented cathode; d, proton exchange membrane; e, voltage sensor; f, plastic frame).

During experiments, all above-mentioned parameters were measured in situ. In experiments 1, 3, 5 (i.e., hydrogen stoichiometry 1.82, 0.91 and 0.55, respectively), the composition and content of the exhaust gas at the anode of the segmented cell were analyzed in situ by gas phase chromatogram (SHIMADAZU GC-14C). All data were focused on the segmented fuel cell.

3. Results and discussion

3.1. Tests under normal operating condition

It has been reported that there is an interfacial potential between metal voltage sensor and proton exchange membrane [16] in our previous work. Thus, pure hydrogen was fed into the anode before experiments. The interfacial potentials between the three metal voltage sensors and reference hydrogen electrode were measured to be all about 0.26 V under open circuit condition. Therefore, the measured potential difference between anode and metal voltage sensor plus 0.26 V could be taken as the interfacial potential between anode and membrane. Meanwhile, since a mixing gas of 73% hydrogen is used as the anode fuel gas, it can be calculated that the reference hydrogen electrode potential in this experiment is ca. 5 mV higher than the potential in pure hydrogen condition. Thus the cathode and anode potentials measured were corrected correspondingly.

Under normal operating condition (experiment 1, total fuel flowrate 800 ml min^{-1}, hydrogen stoichiometry 1.82), the responding processes of current distribution, cell voltage, cathode and anode potentials, and local interfacial potentials between anode and membrane during loading are shown in Fig. 5. It could be seen that before loading, the anode potential is ca. 27 mV when the fuel cell is kept in the open circuit condition (time before 0 s). It indicates that there is certain amount of oxygen permeation within fuel cell, thus causing the anode potential to be higher than the reference hydrogen electrode potential in the open circuit condition. The local interfacial potentials in different regions between anode and membrane are the same, which means that there is no in-plane (along the flowfield) potential difference of the proton exchange membrane at this time. The current distribution in the fuel cell under loading condition is relatively uniform. Among the five segments, the largest current is 9.5 A, and the smallest current is 8.8 A. The fuel cell is steady at 0.7 V. It could also be seen that the anode potential increases slightly to about 50 mV due to the anode polarization after loading. The local interfacial potentials between anode and membrane increase consecutively from fuel inlet to fuel outlet with a value of 48, 51 and 62 mV, respectively. As it is well known, the hydrogen concentration will decrease along the flow direction due to the hydrogen consumption by the electrochemical reaction. Under this normal condition, the hydrogen concentration measured by gas phase chromatogram in the exhaust gas reaches 54.9%, which means that the hydrogen supply is sufficient. Thus the local interfacial potentials between anode and membrane in different regions only differ slightly.

3.2. Tests under fuel starvation conditions

As mentioned before, the hydrogen supply is insufficient under fuel starvation conditions, so water electrolysis and carbon corrosion reaction would take place to compensate for the residual loading current that the hydrogen oxidation reaction could not provide. The changes of current distribution, cell voltage, cathode and anode potentials, and local interfacial potentials between anode and membrane with time under fuel starvation condition (experiment 3, total fuel flowrate 400 ml min^{-1}, hydrogen stoichiometry 0.91) are shown in Fig. 6. As shown in Fig. 6a, the current distribu-
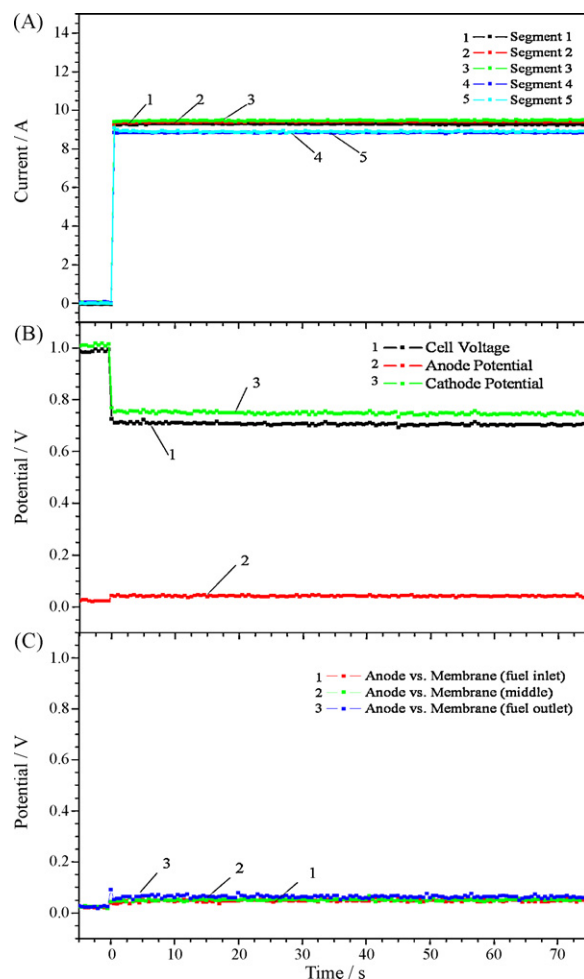

Fig. 5. Under experiment 1 (hydrogen stoichiometry 1.82): (a) the current distribution; (b) the cell voltage and the cathode and anode potentials; (c) the changes of interfacial potentials between anode and membrane with time.

tion is significantly uneven because the hydrogen stoichiometry is only 0.91. The current of Segment 1 increases rapidly after loading, meanwhile the currents of the other four segments all decrease. The closer the segment to the fuel outlet, the earlier the current decreases. After loading for 8 s, the current of Segment 1 fluctuates always above 30 A, with an average current of 33.3 A. The currents of Segments 2–5 are all below 5 A. As shown in Fig. 6b, the anode potential increases promptly to reach about 1.3 V after loading due to the fuel starvation. The cathode potential decreases to be only ca. 0.2 V, which is lower than that under normal condition. This is because that the extreme uneven current distribution increases local current density and accelerates the cathode polarization. The cell voltage decreases gradually and starts to reverse after the 10th second on loading, arriving at about −1.1 V finally. Fig. 6c shows the changes of the local interfacial potentials between anode and membrane with time. It could be seen that the local interfacial potentials between anode and membrane in different regions differ largely. After loading, the local interfacial potential increases firstly near the fuel outlet, then in the middle. The interfacial potentials between anode and membrane in these two regions both reach about 1.8 V, exceeding 1.23 V (the electrode potential required for water electrolysis reaction) greatly. It means that water electrolysis reaction should take place in these two regions. The local interfacial potential near the fuel inlet increases to 1.0 V, smaller than 1.23 V, which shows that the anode reaction near fuel inlet is still hydrogen oxidation reaction. Through analyzing the anode exhaust gas at this time
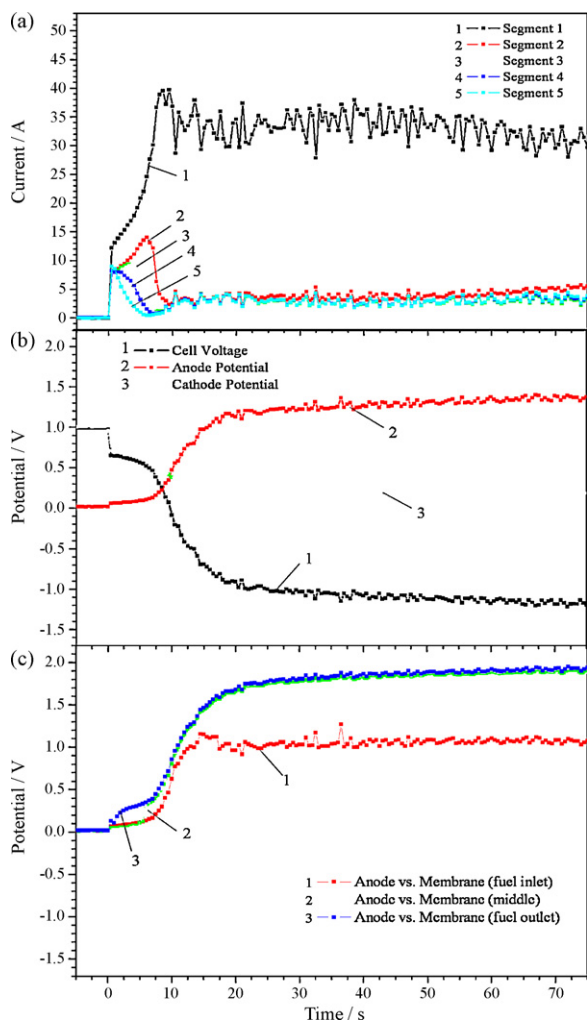
Fig. 6. Under experiment 3 (hydrogen stoichiometry 0.91): (a) the current distribution; (b) the cell voltage and the cathode and anode potentials; (c) the changes of interfacial potentials between anode and membrane with time.

by gas phase chromatogram, it is found that there is no hydrogen in the exhaust gas, and the exhaust gas consists of 71.9% nitrogen, 16.1% oxygen and 12% carbon dioxide.

As shown in the above data, the supply hydrogen stoichiometry is less than 1, so cell reversal would happen due to fuel starvation, and the anode potential would rise. During cell reversal, the local interfacial potentials between anode and membrane in different regions are significantly different, which is because the reactions happening in these regions are not the same due to fuel starvation. In the fuel inlet region, hydrogen oxidation reaction occurs as the existence of hydrogen, so the interfacial potential between anode and membrane in this region is low. While, there is no remaining hydrogen in the middle and the outlet region of the anode as the consumption of hydrogen, so water electrolysis reaction takes place and the interfacial potential between anode and membrane gets higher. The results indicate that there are different local interfacial potentials between anode and membrane in different regions during fuel starvation condition. It is due to the large in-plane resistance of membrane and the different reaction environments in the different regions. It also shows that the anode potential measured by the reference hydrogen electrode is essentially the mixed potential of anode versus membrane in different regions. From the analysis of exhaust gas, water electrolysis reaction is proved to happen at the anode by the oxygen generation. Meanwhile, carbon corrosion is also shown to take place at the anode by the appear-
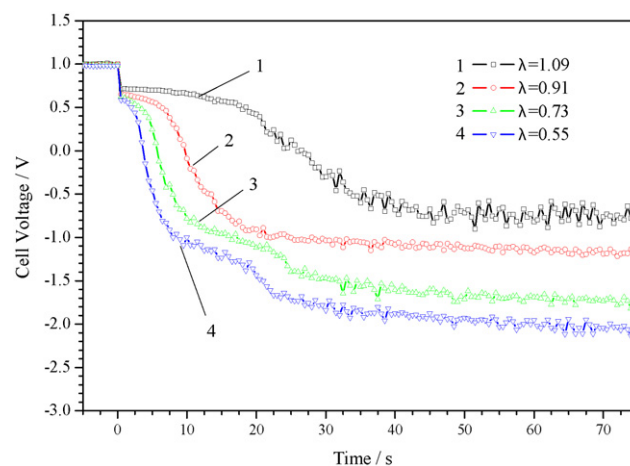

Fig. 7. Changes of the cell voltages with time under the different hydrogen stoichiometries.

ance of carbon dioxide in exhaust gas, which is likely to cause the local degradation of catalyst performance at the anode.

3.3. The influence of hydrogen stoichiometry

The influences of different hydrogen stoichiometries (hydrogen stoichiometry 1.09, 0.91, 0.73 and 0.55) on the cell reversal process due to fuel starvation were investigated respectively in experiments 2–5. Fig. 7 shows the changes of cell voltages with time under different hydrogen stoichiometries. It could be seen that the time needed for cell reversal after loading shortens and the cell reversal voltage reduces as the hydrogen stoichiometry decreases.

Fig. 8 depicts the changes of anode potentials with time under different hydrogen stoichiometries. As it is can be seen, the lower the hydrogen stoichiometry, the faster the anode potential rises after loading and the higher the anode potential reaches. The local interfacial potentials in different regions are significantly different under different hydrogen stoichiometries. The local interfacial potential in the fuel inlet is always less than 1.23 V, which indicates that hydrogen oxidation reaction happens in this region under all mentioned conditions. However, the local interfacial potentials in the middle and the outlet of the anode are both higher than 1.23 V and increase with the decrease of hydrogen stoichiometry. It would even exceed 2.6 V when the hydrogen stoichiometry is 0.55. This indicates that water electrolysis reaction takes place in these regions.
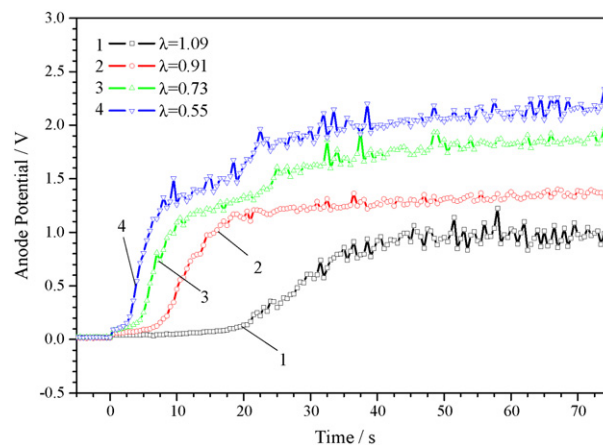

Fig. 8. Changes of the anode potentials with time under the different hydrogen stoichiometries.

Table 2
Cell data under the different hydrogen stoichiometries.

Number	Hydrogen stoichiometry	Time for cell reversal (s)	Cell voltage[a] (V)	Anode potential[a] (V)
2	1.09	26	−0.718	0.955
3	0.91	10	−1.125	1.313
4	0.73	6	−1.689	1.821
5	0.55	4	−1.951	2.058

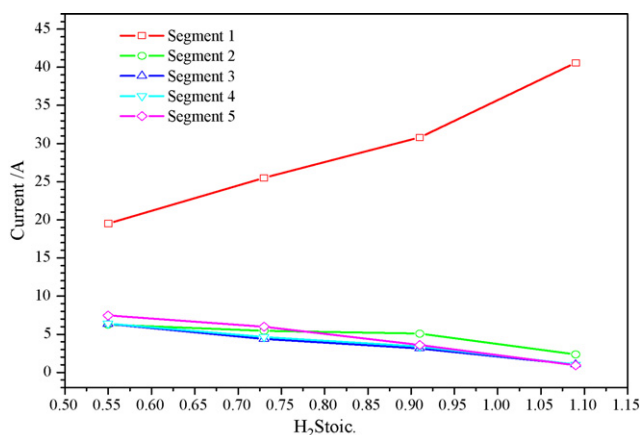[a] The average value during 55–75 s after loading.

Fig. 9. Current distribution conditions under the different hydrogen stoichiometries (the average value during 55–75 s).

The comparison between the cell reversal voltage and the anode potential under different fuel starvation conditions is shown in Table 2.

Fig. 9 shows the current distributions (the average value during 55–75 s) under different hydrogen stoichiometries, respectively. As depicted in Fig. 9, the current of Segment 1 reduces gradually with the decreasing hydrogen stoichiometry while the currents of Segments 2–4 increase gradually. This is because the decrease of hydrogen stoichiometry reduces the current of Segment 1 (hydrogen oxidation current) and correspondingly increases the currents of Segments 2–4 (water electrolysis currents).

The compositions and the contents of the anode exhaust gas under different hydrogen stoichiometries are shown in Table 3.

As can be seen in Table 3, hydrogen is sufficient at the anode under normal operating condition, so there is only hydrogen and nitrogen in the exhaust gas. While under the other two fuel starvation conditions, there is no hydrogen in the exhaust gas. The exhaust gas mainly consists of nitrogen (contained originally in the fuel gas), oxygen and carbon dioxide (generated due to cell reversal). In each experiment, there is no nitrogen consumption at the anode, and the nitrogen flowrate is a constant value. Thus the producing rates of oxygen and carbon dioxide could be calculated under these two starvation conditions. When hydrogen stoichiometry is 0.91, the oxygen producing rate is 24 ml min^{-1} and the carbon dioxide producing rate is 18 ml min^{-1}. When hydrogen stoichiometry is 0.55, the oxygen producing rate is 80 ml min^{-1} and the carbon dioxide producing rate is 20 ml min^{-1}. The results above further show that

the percentage of water electrolysis current to the overall current increases as the decrease of hydrogen stoichiometry. The higher the anode interfacial potential is, the severer the local degradation of the anode catalyst would be.

4. Conclusion

In this research, the fuel starvation conditions of a single cell in a stack were simulated. Through the in situ measurements of current distribution, cell voltage, cathode and anode potentials, as well as local interfacial potentials between anode and membrane of the segmented single cell, the response characteristics of a large area proton exchange membrane fuel cell under different fuel starvation degrees were disclosed.

Experimental results show that the current distribution is significantly uneven under fuel starvation condition. The anode potential rises and the cell voltage reverses. The local interfacial potentials between anode and membrane in different regions differ greatly. In the fuel inlet region, hydrogen oxidation reaction occurs as the existence of hydrogen, and the interfacial potential is lower than 1.23 V. While there is no remaining hydrogen in the middle and the outlet region of the anode as the consumption of hydrogen, so water electrolysis reaction takes place there and the local interfacial potential is significantly higher than 1.23 V. The anode potential measured is essentially the mixed potential of anode versus proton exchange membrane in different regions. The high local interfacial potential at the anode would cause local carbon corrosion reaction and is likely to result in the local catalyst degradation at the anode.

The current distributions under different fuel starvation degrees are all uneven. The percentage of hydrogen oxidation current to the overall current is reduced as the fuel starvation degree increases, and the water electrolysis current is enhanced. As the fuel starvation degree increases, the cell voltage gets lower and the anode potential gets higher. The local interfacial potential also gets higher near the anode outlet, resulting in a larger amount of carbon corrosion. The local interfacial potential near the anode outlet increases from ca. 1.8 to 2.6 V when the hydrogen stoichiometry decreases from 0.91 to 0.55. The producing rate of carbon dioxide also increases from 18 to 20 ml min^{-1}.

Table 3
Contents of the anode exhaust gas under the different hydrogen stoichiometries.

No.	Hydrogen stoichiometry	Anode exhaust gas content (%)			
		Hydrogen	Nitrogen	Oxygen	Carbon dioxide
1	1.82	54.9	45.1	0	0
3	0.91	0	71.9	16.1	12.0
5	0.55	0	39.1	48.7	12.0

References

[1] W. Schmittinger, A. Vahidi, J. Power Source 180 (2008) 1–14.
[2] S.D. Knights, K.M. Colbow, J. St-Pierre, D.P. Wilkson, J. Power Sources 127 (2004) 127–134.
[3] Z. Liu, L. Yang, Z. Mao, et al., J. Power Sources 157 (2006) 166–176.
[4] K. Mitsudo, T. Murahashi, J. Electrochem. Soc. 137 (1990) 3079–3085.
[5] K. Mitsudo, T. Murahashi, J. Appl. Electrochem. 21 (1991) 524–530.
[6] A. Lundblad, P. Bjornbom, J. Electrochem. Soc. 139 (1992) 1337–1342.
[7] R.H. Song, C.S. Kim, D.R. Shin, J. Power Sources 86 (2000) 289–293.
[8] A. Taniguchi, T. Akita, K. Yasuda, Y. Miyazaki, J. Power Sources 130 (2003) 42–49.

[9] M.V. Lauritzen, P. He, A.P. Young, et al., J. New Mater. Electrochem. Syst. 10 (2007) 143–145.

[10] W.R. Baumgartner, P. Parz, S.D. Fraser, J. Power Sources 182 (2008) 413–421.

[11] J. Stumper, S.A. Campbell, D.P. Wilkinson, et al., Electrochem. Acta 43 (1998) 3773.

[12] S.J.C. Cleghorn, C.R. Derouin, M.S. Wilson, et al., J. Appl. Electrochem. 28 (1998) 663.

[13] Z. Liu, Z. Mao, B. Wu, J. Power Sources 141 (2005) 205–210.

[14] X. Yan, M. Hou, et al., J. Power Sources 163 (2007) 966–970.

[15] S. Kim, S. Shimpalee, J.W. Van Zee, J. Power Sources 135 (2004) 110–121.

[16] Q. Shen, et al., J. Power Sources 189 (2009) 1114–1119.